

RSC Advances



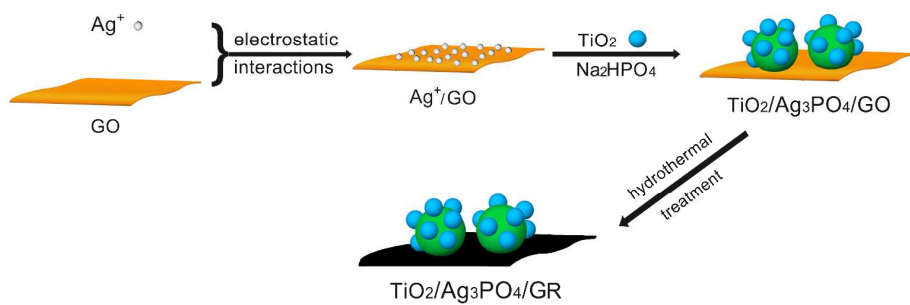
This is an *Accepted Manuscript*, which has been through the Royal Society of Chemistry peer review process and has been accepted for publication.

Accepted Manuscripts are published online shortly after acceptance, before technical editing, formatting and proof reading. Using this free service, authors can make their results available to the community, in citable form, before we publish the edited article. This *Accepted Manuscript* will be replaced by the edited, formatted and paginated article as soon as this is available.

You can find more information about *Accepted Manuscripts* in the [Information for Authors](#).

Please note that technical editing may introduce minor changes to the text and/or graphics, which may alter content. The journal's standard [Terms & Conditions](#) and the [Ethical guidelines](#) still apply. In no event shall the Royal Society of Chemistry be held responsible for any errors or omissions in this *Accepted Manuscript* or any consequences arising from the use of any information it contains.

Graphical Abstract



Schematic representation of synthetic strategy for $\text{TiO}_2/\text{Ag}_3\text{PO}_4/\text{GR}$ composites

Bifunctional TiO₂/Ag₃PO₄/Graphene composites with superior visible light photocatalytic performance and synergistic inactivation of bacteria

Xiaofei Yang,^{a,*} Jieling Qin,^a Yan Jiang,^a Rong Li,^a Yang Li,^a and Hua Tang^{a,*}

^a School of Materials Science and Engineering, Jiangsu University, Zhenjiang 212013, China

Abstract

In this work, bifunctional TiO₂/Ag₃PO₄/graphene (GR) composites have been prepared via the combination of ion-exchange method and hydrothermal approach, the fabrication of “pizza-like” three-phase TiO₂/Ag₃PO₄/GR composites has been achieved through the electrostatic-driven assembly of positively-charged Ag⁺ on negatively-charged graphene oxide (GO) sheets, followed by the nucleation & controlled growth of Ag₃PO₄ and the deposition of Degussa P25 on the GO surface, consequently, the hydrothermal treatment leads to the generation of TiO₂/Ag₃PO₄/GR composites with well-defined structures. The as-prepared composites exhibited highly efficient visible light photocatalytic activity toward organic dye molecule degradation and showed excellent bactericidal performance. This is the first report on the production of bifunctional three-phase metal oxide-Ag₃PO₄-GR composite materials with improved photocatalytic and antibacterial properties. The improved photocatalytic activity is attributed to the effective separation of photoexcited electron-hole pairs and fast charge transfer between components in the composite, while its excellent bactericidal performance is believed to come from intrinsic bacterial inactivation of Ag₃PO₄ and photo-induced antibacterial activity of active oxygen-containing radicals generated in the irradiated system. The proper molar ratio of Ag₃PO₄/TiO₂ and the added amount of GO in the precursor have been considered to play crucial roles in the formation of bifunctional composites with promising properties. The TiO₂/Ag₃PO₄/GR composite significantly decreases the percentage of expensive Ag-containing material while reveals better photocatalytic and antibacterial performance than Ag₃PO₄, providing new insights into the low-cost, large-scale production of Ag₃PO₄-based function materials for practical applications.

* To whom correspondence should be addressed. Tel: 86-511-88790191; Fax: 86-511-88791947

E-mail: xyang@mail.ujs.edu.cn (Dr Yang XF); tanghua@ujs.edu.cn (Dr. Tang H);

1. Introduction

Past few decades have witnessed the increasing environmental pollution and exposures to environmental pollution remain a major source of health risk throughout the world. However, environmental pollution can not be simply generated and pollutants take many forms. They include not only inorganic and organic chemicals, but also bacteria and organisms. Despite the major efforts have been made over the past few years to clean up the environment, the search for new materials and technology to meet present demands in the removal and sterilization of a wide range of pollutants in water becomes even more urgent. Photocatalysis is an effective, economical and environment-friendly photooxidation process where the produced active oxygen-containing radicals are widely used to remove the contaminants by converting them to CO_2 , H_2O ,¹⁻⁵ etc. Recent advances in new photocatalytic materials and nanotechnology have demonstrated that highly efficient solar photocatalytic degradation of organic pollutants and bacteria in the presence of photocatalysts can be achieved, as a result, the design of highly active visible-light-responsive photocatalytic materials has attracted great attention and a range of visible light photocatalysts have been developed for the environmental decontamination.⁶⁻¹³

Most recently, the pioneering work reported by Ye and co-workers has shown that silver orthophosphate (Ag_3PO_4) can achieve a quantum efficiency of nearly 90 % for O_2 evolution from water under visible light irradiation.¹⁴ Moreover, it has been reported that Ag_3PO_4 demonstrates significant visible-light-driven photocatalytic activity in the degradation of organic pollutants in aqueous solution.¹⁵ Compared with several currently known visible light photocatalysts including doped TiO_2 , BiVO_4 , and AgX ($X=\text{Cl}, \text{Br}$), Ag_3PO_4 has a significantly higher photocatalytic efficiency and has been considered to be a promising candidate for practical applications due to its superior photooxidative capabilities by utilizing abundant solar light. However, several limitations of Ag_3PO_4 photocatalytic system may restrict its practical use in energy and environmental sciences. Firstly, the Ag_3PO_4 photocatalyst is unstable upon photo-illumination and it is prone to be photoreduced and decomposed to weakly active Ag, the presence of generated black metallic Ag particles in the photocatalytic system would inevitably prevent visible light absorption and decrease its photocatalytic activity; secondly, the use of a large amount of expensive silver-containing raw material in the present photocatalytic system

strongly limits its large-scale production and practical applications. Furthermore, Ag_3PO_4 normally possesses irregular microstructures and is insoluble in most solvents, the morphology, particle size, and specific highly reactive facet have been proved to play major roles in its highly efficient photocatalytic activity. Most recently, considerable efforts have been made to synthesize Ag_3PO_4 photocatalysts with well-defined morphologies including cubic Ag_3PO_4 microcrystals,¹⁶ hierarchical Ag_3PO_4 porous microcubes,¹⁷ dendritic Ag_3PO_4 ,¹⁸ concave trisoctahedral Ag_3PO_4 microcrystals,¹⁹ Ag_3PO_4 tetrapods²⁰ and to design Ag_3PO_4 -based composite photocatalysts by the combination of Ag_3PO_4 with different materials including metal oxides (TiO_2 ,²¹⁻²³ Fe_3O_4 ,²⁴ SnO_2 ²⁵), Ag,²⁶⁻³⁰ AgX ($X=\text{Cl}$, Br and I),³¹⁻³³ carbon materials such as graphene oxide,³⁴⁻³⁶ carbon quantum dots³⁷ and hydroxyapatite.^{38,39} Despite tremendous efforts, it is still urgent and highly desirable to develop a facile and low-cost process for the large-scale production of Ag_3PO_4 -based photocatalysts with enhanced stability and highly efficient photocatalytic activity.

Degussa P25, a commercially available TiO_2 nanomaterial, consists of two crystal forms of approximately 20 % rutile and 80 % anatase and has been widely used in the photocatalytic study due to its low cost, photocatalytic activity, stability and innocuousness. However, its visible-light-driven photocatalytic efficiency is generally low due to its wide band gap and the fact that it only absorbs lights in the ultraviolet region. Yao and co-workers reported the synthesis of heterostructured $\text{Ag}_3\text{PO}_4/\text{TiO}_2$ photocatalysts by the deposition of Ag_3PO_4 nanoparticles onto the P25 surface *via* an *in-situ* precipitation method,²¹ the obtained composite photocatalyst showed significantly improved photocatalytic degradation of organic dyes than pure Ag_3PO_4 and TiO_2 , a better structural stability and recyclability of the photocatalyst under visible light irradiation were also observed.

Chemically derived graphene oxide (GO) with oxygen-containing functional groups has been proved to be a promising candidate for the construction of composite photocatalysts due to its solubility in solvents and its negatively-charged active sites on its high-surface-area sheets. Our previous report and other groups' work^{34-36,40} confirm that the hybridization of Ag_3PO_4 with GO sheets not only results in the enhancement in the visible light absorption, but also leads to an improved visible light photocatalytic performance since GO sheets could facilitate charge transfer and suppress the recombination of photo-generated electrons and holes in the photocatalytic system. Our study further

demonstrates the generation of the $\text{Ag}_3\text{PO}_4/\text{GR}$ composite photocatalyst by the hydrothermally treatment of the $\text{Ag}_3\text{PO}_4/\text{GO}$ composite causes an obvious increase in its visible light photocatalytic activity.⁴¹

In consideration of the facts that improved stability, enhanced photocatalytic performance and low-cost of Ag_3PO_4 materials are all important factors responsible for stable and highly efficient Ag_3PO_4 -based visible light photocatalysts. Herein, for the first time, we develop an efficient strategy for the fabrication of $\text{TiO}_2/\text{Ag}_3\text{PO}_4/\text{GR}$ composites where the presence of TiO_2 and GR in the composite may effectively reduce the cost for the preparation of the composite while the hybridization of photocatalytic P25 and Ag_3PO_4 on highly conductive GR sheets favors the separation of photo-induced electrons and holes as well as charge transfer in the three-phase composite photocatalyst. The morphology, size, and visible-light photocatalytic behavior of the composites are investigated together with their structural and physicochemical properties. Furthermore, the $\text{TiO}_2/\text{Ag}_3\text{PO}_4/\text{GR}$ composites are believed to have intrinsic antibacterial activity and enhanced photo-induced inactivation of bacterial cells under visible light irradiation. To the best of our knowledge, this is the first report concerning the fabrication of bifunctional Ag_3PO_4 -based composites with improved visible light photocatalytic performance and enhanced antibacterial activity. The investigation provides a low-cost and effective approach for the large-scale production of Ag_3PO_4 -based functional composite materials for the efficient removal of organic contaminants and bacteria inactivation under visible light irradiation.

2. Experimental section

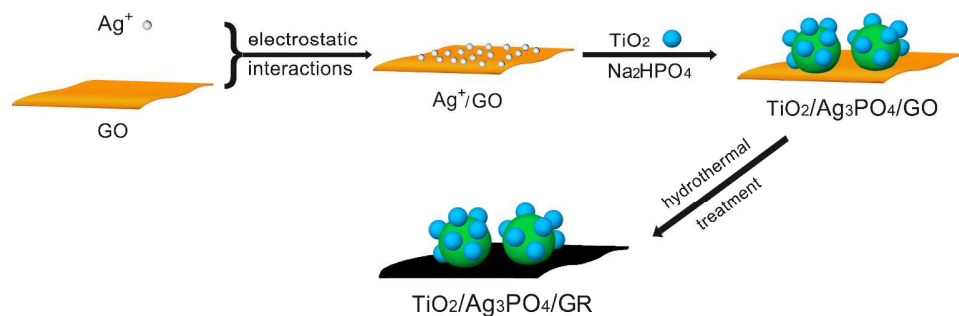
2.1 Synthesis of samples

All reagents was purchased from Sinophram Chemical Reagent Co. Ltd. (Shanghai, China) and used as received without further purification. Graphite oxide was synthesized from natural graphite by a modified Hummers' method with additional KMnO_4 .^{42,43} In a typical synthesis, the as-synthesized graphite oxide was firstly dispersed in distilled water, followed by ultrasonication for several hours to give GO dispersions. Then AgNO_3 solution was added into the above GO solution under magnetic stirring. After gently stirring overnight, the ultrasonicated Degussa P25 aqueous dispersion was added

dropwise into the Ag^+ -GO mixture, the mixed solution was stirred for further 30 min, followed by the addition of Na_2HPO_4 aqueous solution into the P25- Ag^+ -GO mixture. Upon the addition of Na_2HPO_4 , yellowish-brown product precipitates were formed instantaneously. The reaction solution was then transferred into a 100 mL Teflon-lined stainless steel autoclave and kept in an oven at 180 °C for 24 h. The autoclave was left to cool naturally to room temperature; the obtained precipitate was collected by centrifugation, washed several times with deionized water and absolute ethanol, and dried at 60 °C under vacuum overnight. The reaction conditions for the preparation of hydrothermal composites are shown in Table 1 and the overall synthetic procedure for the generation of $\text{TiO}_2/\text{Ag}_3\text{PO}_4/\text{GR}$ composites is illustrated in Scheme 1. Samples S1, S0.8, S0.6, S0.4, S0.2 represents the samples prepared by using different molar ratios of $\text{Ag}_3\text{PO}_4/\text{TiO}_2$ while samples S-0, S-5, S-10, S-20, S-50, S-100 stands for composites obtained in the presence of different GO amounts.

Table 1. Reaction conditions for the preparation of hydrothermal products

Sample	GO	AgNO_3	P25	$\text{Na}_2\text{HPO}_4 \cdot 7\text{H}_2\text{O}$	$M(\text{Ag}_3\text{PO}_4/\text{TiO}_2)$
S0	20 mg	9 mmol, 1.53 g		3 mmol, 0.804 g	
S1	20 mg	9 mmol, 1.53 g	3 mmol, 0.24 g	3 mmol, 0.804 g	1
S0.8	20 mg	9 mmol, 1.53 g	3.75 mmol, 0.3 g	3 mmol, 0.804 g	0.8
S0.6	20 mg	9 mmol, 1.53 g	5 mmol, 0.4 g	3 mmol, 0.804 g	0.6
S0.4	20 mg	9 mmol, 1.53 g	7.5 mmol, 0.6 g	3 mmol, 0.804 g	0.4
S0.2	20 mg	9 mmol, 1.53 g	15 mmol, 1.2 g	3 mmol, 0.804 g	0.2
S-0		9 mmol, 1.53 g	3.75 mmol, 0.3 g	3 mmol, 0.804 g	0.8
S-5	5 mg	9 mmol, 1.53 g	3.75 mmol, 0.3 g	3 mmol, 0.804 g	0.8
S-10	10 mg	9 mmol, 1.53 g	3.75 mmol, 0.3 g	3 mmol, 0.804 g	0.8
S-20	20 mg	9 mmol, 1.53 g	3.75 mmol, 0.3 g	3 mmol, 0.804 g	0.8
S-50	50 mg	9 mmol, 1.53 g	3.75 mmol, 0.3 g	3 mmol, 0.804 g	0.8
S-100	100	9 mmol, 1.53 g	3.75 mmol, 0.3 g	3 mmol, 0.804 g	0.8



Scheme 1. Schematic illustration of the formation of TiO₂/Ag₃PO₄/GR composites.

2.2 Characterization

The morphologies of the as-synthesized products were examined by field-emission scanning electron microscopy (FESEM, JEOL, JSM-7001F), transmission electron microscopy (TEM, JEOL, JEM-2100) and atomic force microscopy (AFM, MFP-3D SA). The phases of the obtained products were collected on a Bruker D8 Advance X-ray diffractometer (Cu K α radiation, $\lambda = 0.15406 \text{ \AA}$) in a 2θ range from 10° to 80° at room temperature. Raman experiments were performed using a DXR spectrometer using the 532 nm laser line and measurements were made in backscattering geometry. UV-Visible diffuse reflectance spectra were recorded on within 200-800 nm wavelength range using a Shimadzu UV2450 spectrometer.

2.3 Photocatalytic experiments

The photocatalytic activities of products were valued by the decomposition of organic dyes under visible-light irradiation. The optical system for the photocatalytic reaction was composed of a 350 W Xe lamp and a cut-off filter ($\lambda > 420 \text{ nm}$). Organic dye solutions (100 mL, 10^{-5} mol/L) containing 50 mg of samples were put in a sealed glass beaker and first ultrasonicated for 10 min, and then stirred in the dark for 30 min to ensure absorption-desorption equilibrium. After visible light illumination, 4 mL of samples were taken out at regular time intervals (2 min) and separated through centrifugation (10000 rpm, 10 min). The supernatants were analyzed by recording variations of the absorption band maximum in the UV-Vis spectra of the dye molecule by using a Lambda 25 UV/Vis spectrophotometer.

2.4 Evaluation on antibacterial activities of samples

Bacteria was cultivated in nutrient broth at 37 °C for 18 h in a rotary shaker until reaching stationary growth phase. The as-prepared cells were then resuspended and diluted to the required cell density of around 10^7 colony-forming units per milliliter (CFU/mL) with sterilized saline solution (0.9% NaCl). The antibacterial activity of the composites was tested on six bacterial strains *Escherichia coli*, *Staphylococcus aureus*, *Salmonella typhi*, *Pseudomonas aeruginosa*, *Bacillus subtilis*, *Bacillus pumilus* from ATCC. All of the bactericidal experiments were performed at room temperature and repeated three times in order to give an average value; the measured data for each set of experiments were expressed with the mean and standard deviation.

The minimum inhibitory concentrations (MIC) of each of composites were determined against all test strains. Various concentrations (6.25 ppm, 12.5 ppm, 25 ppm, 50 ppm, 100 ppm, 200 ppm) of the composites were mixed with freshly sterilized (121°C, 15 min) and nutrient broth (tempered at 37 °C) in glass tubes (15 mm×15 mm), consequently 100 µL of pre-cultured strain (initial concentration 10^6 CFU/mL) was added into each tube by micropipette. All the tubes were then placed in a precision constant temperature incubator at 35 °C for 48 h where a high-pressure mercury lamp (Philips HPR 125 W) was used as light source. MIC was determined as the lowest composite concentration that resulted in complete inhibition in nutrient broth. For the minimum bactericidal concentration (MBC), the mixtures of a series of concentrations (MIC, 2MIC, 4MIC, ...) of composite dispersions with test strains were drawn with one loop full streak-inoculated to the nutrient agar plates, respectively. All the plates were then placed in the same incubator equipped with the same light source at 35 °C for 48 h. MBC was determined as the lowest composite concentration that appeared without any colonies could be observed on the plates.

In order to further investigate the effect of the antibacterial composite on the bacteria cells, the best sample S0.8 was chosen as the best antibacterial composite from the MIC and MBC results and the colonies were counted to determine the viable bacterial numbers after being incubated. In a typical process, PBS buffer was first prepared from a mixture of 0.2 M NaH_2PO_4 and 0.2 M Na_2HPO_4 aqueous solutions, S0.8 dispersion with the concentration of 200 ppm was then mixed with sterilized PBS solution, followed by the addition of pre-cultured strain to reach the cell concentration of 10^6 CFU/mL.

All the tubes were then incubated in a temperature-controlled rotary shaker at 20 °C for different times (0, 0.5 h, 1 h, 2 h, 4 h, 8 h). For TEM characterizations of untreated and treated samples, 10 μL of each specimen dispersion was first loaded on TEM copper grids and was then stained with tungstophosphoric acid aqueous solution. The air-dried copper grids were examined using the TEM (JEOL JEM-2100) as described earlier.

3. Results and Discussion

The morphological features of $\text{TiO}_2/\text{Ag}_3\text{PO}_4/\text{GR}$ composites were evaluated by SEM, TEM and HRTEM characterization and the results are shown in Fig. 1. SEM observations shown in Fig. 1a and Fig. 1b reveal the formation of pizza-like composite structures, the agglomeration of micro-sized Ag_3PO_4 particles and TiO_2 nanoparticles was observed on the surface of graphene sheets. Two distinct particles were found in the high-magnification SEM image of the composite shown in Fig. 1b, larger particles ranging from 0.3 μm to 0.8 μm are assigned to as-prepared Ag_3PO_4 crystals and smaller nanoparticles are attributed to hydrothermally treated Degussa P25. Moreover, the EDX pattern of $\text{TiO}_2/\text{Ag}_3\text{PO}_4/\text{GR}$ composites was also recorded and shown in Fig. 1b (inset), showing the presence of several signals from Ti, Ag, P, C and O. The corresponding TEM image of the $\text{TiO}_2/\text{Ag}_3\text{PO}_4/\text{GR}$ composites was shown in Fig. 1c and Fig. S1 where the particle size characteristics of each component is clearly identified, irregular micro-sized Ag_3PO_4 particles and smaller TiO_2 nanoparticles were found to be covered by thin graphene sheet. In addition, a HRTEM image was recorded on the selected area of Fig. 1c and the high-magnification observation shown in Fig. 1d and Fig. S1 clearly confirms the presence of thin and wrinkled graphene layers, the interplanar spacing of 0.35 nm was clearly determined, which corresponds to (101) crystallographic plane of TiO_2 , in good agreement with anatase TiO_2 (JCPDS No. 21-1272).

Fig. 2a shows the XRD pattern of as-synthesized $\text{TiO}_2/\text{Ag}_3\text{PO}_4/\text{GR}$ composites. Two diffraction peaks marked by “•” can be readily indexed as the (101) and (211) planes of anatase (JCPDS No. 21-1272) and the rest of diffraction peaks can be identified to the body-centered cubic phase of Ag_3PO_4 (JCPDS No. 06-0505). No obvious characteristic diffraction peaks of GR or GO are observed in the XRD pattern of $\text{TiO}_2/\text{Ag}_3\text{PO}_4/\text{GR}$ composites. The phenomenon might be ascribed to low diffraction intensities of GR and GO compared to those of crystalline Ag_3PO_4 and TiO_2 , as well as the tiny amount

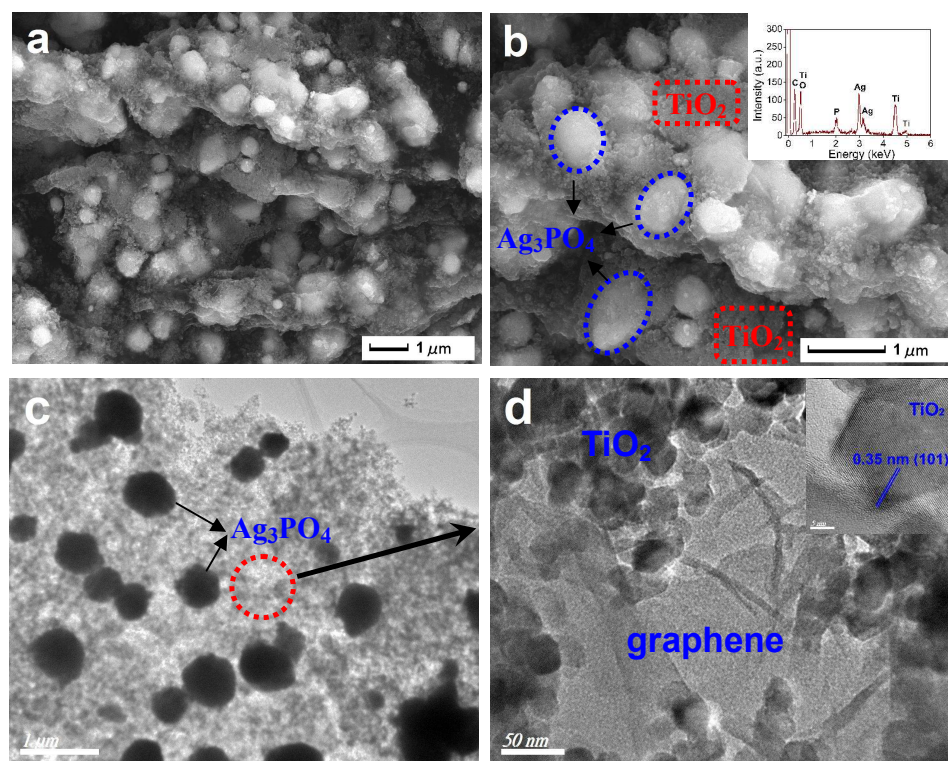


Fig. 1 SEM images (a, b, EDX inset) and TEM images (c, d, HRTEM inset) of as-prepared $\text{TiO}_2/\text{Ag}_3\text{PO}_4/\text{GR}$ composites

graphene oxide employed in the reactants. It is well-known that Raman spectroscopy plays an important role in determining the detailed structure of graphitic materials, thus Raman spectra of GO, Ag_3PO_4 , as-synthesized $\text{TiO}_2/\text{Ag}_3\text{PO}_4/\text{GR}$ composites were recorded. Two distinct bands at 1355 cm^{-1} and 1595 cm^{-1} are observed in the Raman spectrum of GO (Fig. S2a), corresponding to the D and G bands of graphite, respectively. Several characteristic bands corresponding to the vibrations of Ag_3PO_4 (Fig. S2b) appear in the region less than 1200 cm^{-1} , which can be assigned to different modes of Ag_3PO_4 sample including the external modes, the bending vibration of the tetrahedral PO_4 ionic group, the symmetric stretch of P-O-P and O-P-O bonds. It can be seen from Fig. 2b that the spectrum of the composite also exhibits two peaks at around 1350 cm^{-1} (D band) and 1590 cm^{-1} (G band), moreover, other peaks ranging from $100\text{--}1200\text{ cm}^{-1}$ are believed to come from Ag_3PO_4 and TiO_2 . Generally, the intensity ratio of the D and G bands (I_D/I_G) is applied to evaluate the disorder degree in the graphitic layers and average size of the sp^2 domains of the graphitic materials, the I_D/I_G value of GO is estimated to be about 0.92, while an increased I_D/I_G value ratio of 1.05 was observed in the $\text{TiO}_2/\text{Ag}_3\text{PO}_4/\text{GR}$

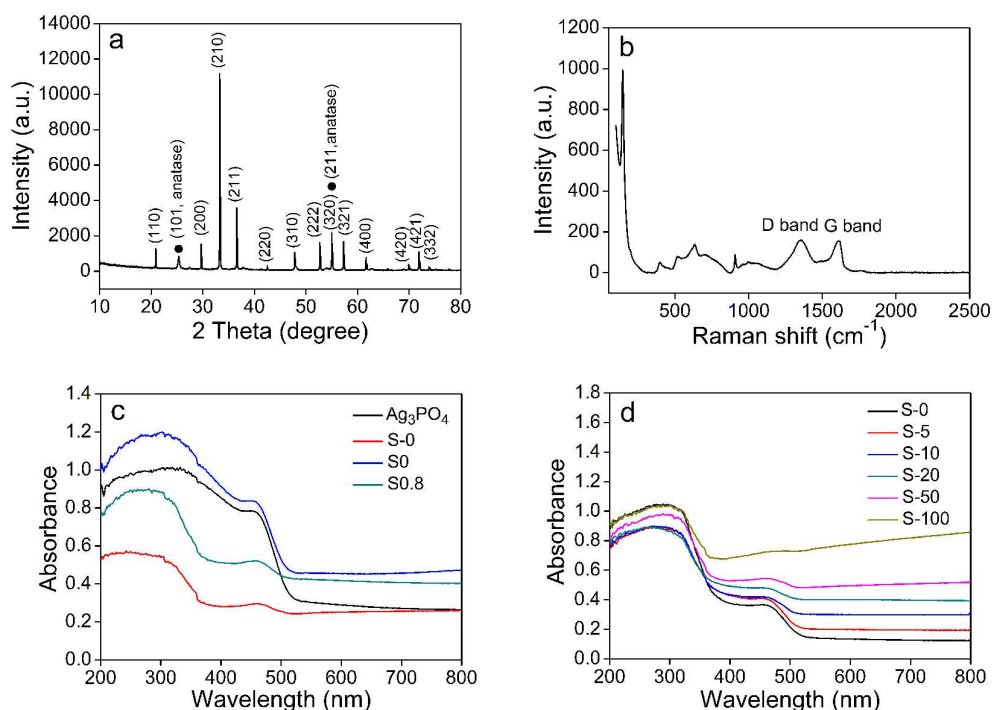


Fig. 2 XRD pattern (a) and Raman spectra (b) of $\text{TiO}_2/\text{Ag}_3\text{PO}_4/\text{GR}$ hybrids; UV-vis diffuse reflectance spectra of different photocatalyst (c) and different amount of GO as precursors(d).

composite, indicating that less defects formed in the graphitic layers, which suggests the reduction of GO to GR upon hydrothermal treatment in the composite.

It is believed that visible light absorption properties of catalysts are crucial in determining their photocatalytic performance, especially for the photocatalytic pollutant or bacteria degradation under visible light irradiation. Thus diffuse reflectance spectra of different samples were recorded and are shown in Fig. 2c. It is notable that pure Ag_3PO_4 showed good absorbance in the whole region, the hybridization of Ag_3PO_4 with P25 (S-0) resulted in the obvious decrease in the absorbance, whereas the introduction of 20 mg GO in precursors (S0) caused a slight increase in the absorbance. The $\text{TiO}_2/\text{Ag}_3\text{PO}_4/\text{GR}$ composite S0.8 where 20 mg GO is employed and the molar ratio of $\text{Ag}_3\text{PO}_4/\text{TiO}_2$ is 0.8 exhibited a better absorbance than pure Ag_3PO_4 in the visible range (500-800 nm) and the composite S-0 in the whole UV-visible range, however, its absorbance is obviously lower than that of S0 sample where 20 mg GO is incorporated with Ag_3PO_4 in the absence of P25, implying that the introduction of GO into the composite definitely favors the enhanced visible light absorbance while the

employment of TiO_2 has a negative effect on the visible light absorbance of the composite. It is also shown from Fig. 2d that the presence of different amounts of GO in the precursor affects the optical property of light absorption for the $\text{TiO}_2/\text{Ag}_3\text{PO}_4/\text{GR}$ obviously, the added GO has been reduced to GR upon the hydrothermal treatment by losing the majority of functional groups and the generated GR induces the increased light absorption intensity particularly in the visible region, as observed in all of six composites (S-0, S-5, S-10, S-20, S-50, S-100, S-200) with different addition amounts of GO. The presence of GR in the composites leads to a continuous absorption band in the visible light region, which is in good agreement with the color of the samples.

The photocatalytic activities of $\text{TiO}_2/\text{Ag}_3\text{PO}_4/\text{GR}$ composites were first evaluated by decomposing of RhB under visible light irradiation. It is clearly shown from Fig. 3a that the sample S0 ($\text{Ag}_3\text{PO}_4/\text{GR}$ composite) exhibits the lowest photocatalytic activity of less than 80 % in 12 min, when 0.24 g TiO_2 was introduced into the $\text{Ag}_3\text{PO}_4/\text{GR}$ composite, the corresponding three-phase composite S1 showed enhanced photocatalytic activities of more than 95 % in 12 min, further addition of TiO_2 leads to the decrease in the molar ratio of $\text{Ag}_3\text{PO}_4/\text{TiO}_2$ from 1 to 0.8, resulting into the generation of the $\text{TiO}_2/\text{Ag}_3\text{PO}_4/\text{GR}$ composite (S0.8) with the highest photocatalytic activity of around 95 % in 6 min and almost 100 % in 10 min. However, $\text{TiO}_2/\text{Ag}_3\text{PO}_4/\text{GR}$ composites with lower molar ratios of $\text{Ag}_3\text{PO}_4/\text{TiO}_2$ than 0.8 (S0.6, S0.4, S0.2) showed decreased photocatalytic efficiencies, all the three-phase $\text{TiO}_2/\text{Ag}_3\text{PO}_4/\text{GR}$ composites demonstrate higher photocatalytic performance than the two-phase $\text{Ag}_3\text{PO}_4/\text{GR}$ composite (S0). The above results imply that the proper molar ratio of $\text{Ag}_3\text{PO}_4/\text{TiO}_2$ plays a crucial role in determining photocatalytic activities of $\text{TiO}_2/\text{Ag}_3\text{PO}_4/\text{GR}$ composites. Furthermore, when the optimal molar ratio of $0.8\text{Ag}_3\text{PO}_4/\text{TiO}_2$ is fixed, the effect of added GO on photocatalytic activities of $\text{TiO}_2/\text{Ag}_3\text{PO}_4/\text{GR}$ composites was investigated and the results are shown in Fig. 3b. The $\text{Ag}_3\text{PO}_4/\text{TiO}_2$ composite (S-0) reveals the photocatalytic efficiency of around 75 % in 12 min in the absence of GO, when 5 mg GO was introduction in the $\text{Ag}_3\text{PO}_4/\text{TiO}_2$ composite, the photocatalytic activity of the composite S-5 was increased to nearly 85 % in 12 min, further increase of GO to 10 mg leads to an enhanced photocatalytic activity of more than 95 % in 12 min. The highest photocatalytic efficiency of around almost 100 % in 10 min was achieved when 20 mg GO was used. However, the addition of a higher amount than 20 mg GO (50 mg, 100 mg) causes negative effect

on the photocatalytic activity of the $\text{TiO}_2/\text{Ag}_3\text{PO}_4/\text{GR}$ composite, photocatalytic efficiencies of two samples (S-50 and S-100) are even lower than that of two-phase $\text{Ag}_3\text{PO}_4/\text{TiO}_2$ composite (S-0), implying the appropriate added GO amount also affects the photocatalytic performance of $\text{TiO}_2/\text{Ag}_3\text{PO}_4/\text{GR}$ composites significantly and the best added GO amount in this study is 20 mg.

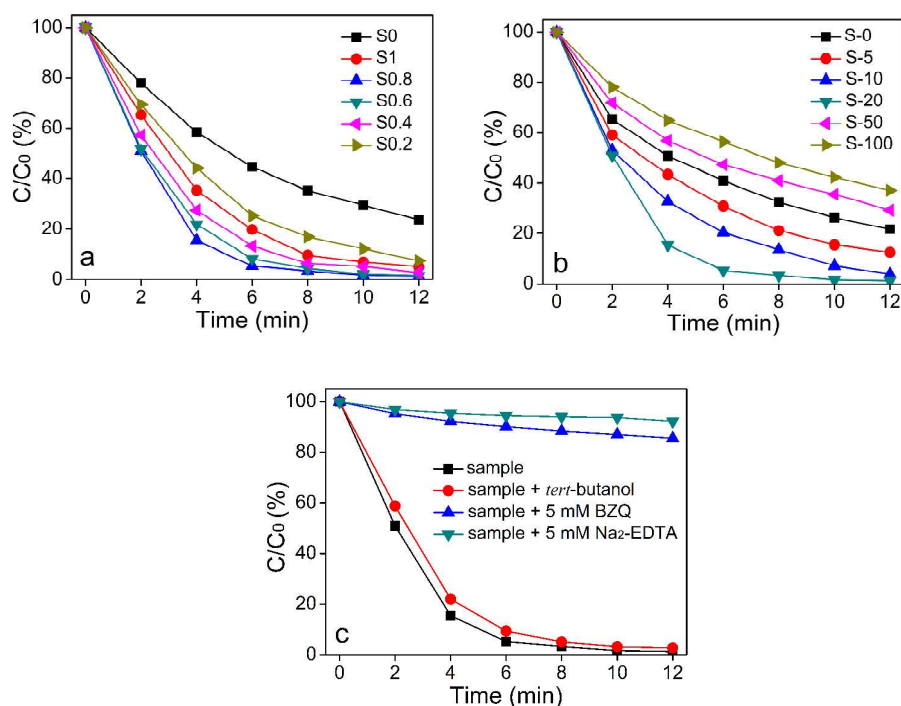


Fig. 3 Visible light photocatalytic activities of $\text{TiO}_2/\text{Ag}_3\text{PO}_4/\text{GR}$ composites with different molar ratios (a) and different added amounts of GO (b) toward RhB; reactive species trapping experiments (c)

Furthermore, reactive species trapping experiments were performed to investigate active oxidizing species in the photocatalytic process where three different chemicals p-benzoquinone (BZQ, a $\text{O}_2^{\cdot -}$ radical scavenger), disodium ethylenediaminetetraacetate (Na_2EDTA , a hole scavenger) and *tert*-butanol (a $\cdot\text{OH}$ radical scavenger) were employed. The experimental results (Fig. 3c) indicated that 5 mM $\text{Na}_2\text{-EDTA}$ as well as 5 mM BZQ was introduced to the above photocatalytic system, the photocatalytic activity of the hybrids was intensively suppressed with the degradation efficiency decreasing from 100 % to 20 % in 10 minutes. Whereas the presence of *tert*-butanol in the $\text{TiO}_2/\text{Ag}_3\text{PO}_4/\text{GR}$ photocatalytic system showed negligible effect on its excellent photocatalytic activity.

The reactive species trapping results indicate that the photo-induced active holes and superoxide ions make major contributions to the highly efficient photocatalytic performance. In addition to the photocatalytic performance toward RhB, two organic dyes MB and MO were also chosen as model pollutants to evaluate the photocatalytic efficiency of the as-prepared TiO₂/Ag₃PO₄/GR photocatalyst and the result was shown in Fig. S3. It can be clearly seen that, when MB was employed, a relatively higher photocatalytic efficiency was observed, while an obvious lower photocatalytic activity was achieved when MO was introduced. It is suggested that the removal of the majority of organic pollutants RhB or MB under visible light irradiation was obtained in 6 min, a longer irradiation time contributes less to its photocatalytic efficiency. However the elimination of organic pollutant MO was found to occur gradually at regular intervals of 2 min, achieving a photocatalytic efficiency of around 60 % in 6 min and almost 100 % in 12 min.

It is well-known that Ag-based materials are effective biocides against numerous kinds of bacteria and fungi, besides, photo-generated oxidative radicals from irradiated TiO₂-based materials are capable of inhibiting the growth of bacteria in the photocatalytic process. Thus, it is reasonable to assume that the obtained TiO₂/Ag₃PO₄/GR composite could be a promising candidate for the disinfection of water by synergistic effects from photocatalytic inactivation of microorganisms and direct bacteria inhibition/killing. For the first time, the intrinsic antibacterial and photocatalytic disinfection of different composite materials were investigated, minimum inhibitory concentration (MIC) and minimum bactericidal concentration (MBC) of different samples under light irradiation are shown in Table 2. It is clearly shown that six samples with different molar ratios (Ag₃PO₄/TiO₂) all exhibited excellent bacteria inhibition activities against four different bacteria, MIC values against *S. aureus*, *S. typhi* and *P. aeruginosa* are observed to be lower than 100 ppm while a relatively higher value of 100 ppm are found against *E. coli*. The bactericidal activities of the above samples are further confirmed by MBC test results, notably, the majority of bacteria can be completely killed in a concentration equivalent to MIC value, implying that the bacteria can be killed simultaneously soon after the growth has been inhibited. When the amount of GO was changed in the precursor where the molar ratio of molar ratio of Ag₃PO₄/TiO₂ was kept at 0.8, six samples still demonstrate excellent antibacterial

activities against four bacteria, similar lower MIC and MBC values against three bacteria *S. aureus*, *S. typhi* and *P. aeruginosa* were obtained while *E. coli* is still an exception. With the increase in the added amount of GO in the precursor from 0 to 5 mg, 10 mg, 20 mg respectively, MIC or MBC of the corresponding sample against three bacteria was observed to be further decreased to a lower value, indicating the introduction of increased amount of GO causes the enhanced bacteria inhibition or bactericidal activity of the sample. However, when more than 20 mg GO was employed into the precursor, as-prepared $\text{TiO}_2/\text{Ag}_3\text{PO}_4/\text{GR}$ composites exhibit a bit worse bacteria inhibition or bactericidal activity toward three bacteria, implying the presence of higher percentage of GR reduced from GO upon hydrothermal treatment has a negative effect on the antibacterial activity of the $\text{TiO}_2/\text{Ag}_3\text{PO}_4/\text{GR}$ composite. It is generally accepted that the direct bacterial activity of Ag_3PO_4 should result from dissolved Ag^+ and the photocatalytic inactivation of bacteria also makes a major contribution to excellent antibacterial performance of $\text{TiO}_2/\text{Ag}_3\text{PO}_4/\text{GR}$ composites. Under visible light irradiation, the synergistic effects from Ag^+ and photo-induced oxidative species lead to total and efficient bacterial removal. For the $\text{TiO}_2/\text{Ag}_3\text{PO}_4/\text{GR}$ samples prepared from precursors with

Table 2. MIC and MBC results of as-prepared composites

Sample	MIC (MBC)			
	<i>E. coli</i>	<i>S. aureus</i>	<i>S. typhi</i>	<i>P. aeruginosa</i>
S0	100 (100)	50 (50)	6.25 (6.25)	6.25 (12.5)
S1	100 (100)	12.5 (25)	6.25 (12.5)	12.5 (12.5)
S0.8	100 (100)	6.25 (12.5)	6.25 (12.5)	12.5 (12.5)
S0.6	100 (100)	12.5 (25)	12.5 (12.5)	12.5 (25)
S0.4	100 (100)	25 (50)	25 (25)	12.5 (50)
S0.2	100 (100)	50 (50)	50 (50)	25 (50)
S-0	100 (100)	50 (100)	25 (50)	25 (25)
S-5	100 (100)	50 (50)	25 (25)	12.5 (25)
S-10	100 (100)	25 (12.5)	12.5 (25)	12.5 (12.5)
S-20	100 (100)	6.25 (12.5)	6.25 (12.5)	12.5 (12.5)
S-50	100 (100)	25 (25)	25 (50)	25 (25)
S-100	100 (100)	25 (50)	50 (50)	25 (50)

different amounts of GO, it is proposed that the proper addition of GO in the precursor may improve the solubility/dispersibility of the sample, which favors membrane penetration of the antibacterial composite into the host cell and leads to inactivation of bacteria more efficiently. However, further increase in the added amount of GO in the precursor results in a higher percentage of reduced GR in the TiO₂/Ag₃PO₄/GR composite, due to the fact that GR only presents limited antibacterial activity, consequently the TiO₂/Ag₃PO₄/GR composite with a higher percentage of GR demonstrates decreased bacteria inhibition or bactericidal effects.

On the basis of above photocatalytic and antibacterial results, the TiO₂/Ag₃PO₄/GR sample S0.8 where the added GO was 20 mg and the molar ratio of Ag₃PO₄/TiO₂ was 0.8 has been evaluated as the best three-phase composite with highly efficient photocatalytic performance and excellent antibacterial activities. In order to further understand synergistic effects of the the TiO₂/Ag₃PO₄/GR composite S0.8, control experiments including MIC (MBC) of the composite S0.8 with *E. coli* in dark, *E. coli* under the light irradiation, mixtures of S0.8 with *E. coli* under the light irradiation were conducted and results are shown in Table 3.

Table 3. MIC and MBC results of control experiments against

Sample	MIC (MBC)					
	S0.8 with <i>E. coli</i> in dark		<i>E. coli</i> under the light		S0.8 with <i>E. coli</i> under the light	
<i>E. coli</i>	> 800	(> 800)	> 800	(> 800)	100	(100)
<i>S. aureus</i>	> 800	(> 800)	> 800	(> 800)	6.25	(12.5)
<i>S. typhi</i>	> 800	(> 800)	> 800	(> 800)	6.25	(12.5)
<i>P. aeruginosa</i>	> 800	(> 800)	> 800	(> 800)	12.5	(12.5)

Furthermore, the determination of rapidity and bactericidal duration of the sample S0.8 has been assessed by time-kill analysis. It is shown from Fig. 4 that treatment with 200 ppm aqueous dispersion of S0.8 demonstrated strong bactericidal effect on different kinds of bacteria considerably, within first 2 h the bacterial population was observed to decrease dramatically from above 6-6.5 log CFU/mL of the control to 2.1-2.4 log CFU/mL for *S. aureus* and *B. subtilis*, around 1.0 log CFU/mL for *P. aeruginosa* and *B. pumilius*, respectively. When the time was prolonged to 4 h, bacterial counts continue to decrease and the number of cells of all bacteria fluctuated around 1 log CFU/mL. After 8 h, the bacterial population was completely inactivated and the data wasn't listed in Fig. 4.

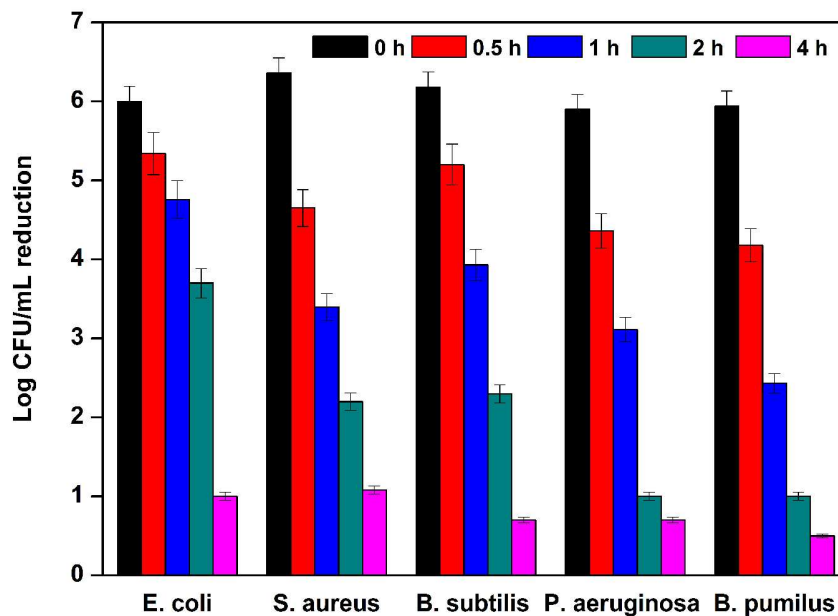


Fig. 4 Time-kill analysis of the composite S0.8 against different bacteria

Furthermore, TEM characterization was used to investigate the morphology changes of typical Gram-negative bacteria *E. coli* and Gram-positive bacteric *S. aureus* cells before and after the disinfection reaction. As shown in Fig. 5a and Fig. 5c, the *E. coli* and *S. aureus* cells remained in a good state in the absence of the antibacterial sample S0.8. However, when the composite was introduced into the system and the composite-bacteria mixture was incubated, it is shown from Fig 5b and Fig. 5d that obvious cell damages or membrane deformation could be observed for both two bacteria, in which regular rod-like or spherical cellular shapes, as well as bigger cell sizes are found to disappear. TEM observations imply that the $\text{TiO}_2/\text{Ag}_3\text{PO}_4/\text{GR}$ composite may react with membrane proteins to damage the cell membrane, resulting in the inactivation of its relative function. It is suggested that the addition of GO in the precursor not only improved the solubility of the composite in antibacterial experiments, the high-surface-area GR sheet reduced from GO could also adsorb and gather the bacteria onto its surface, resulting in enhanced interactions between bacteria and active bactericidal components on GR sheets.

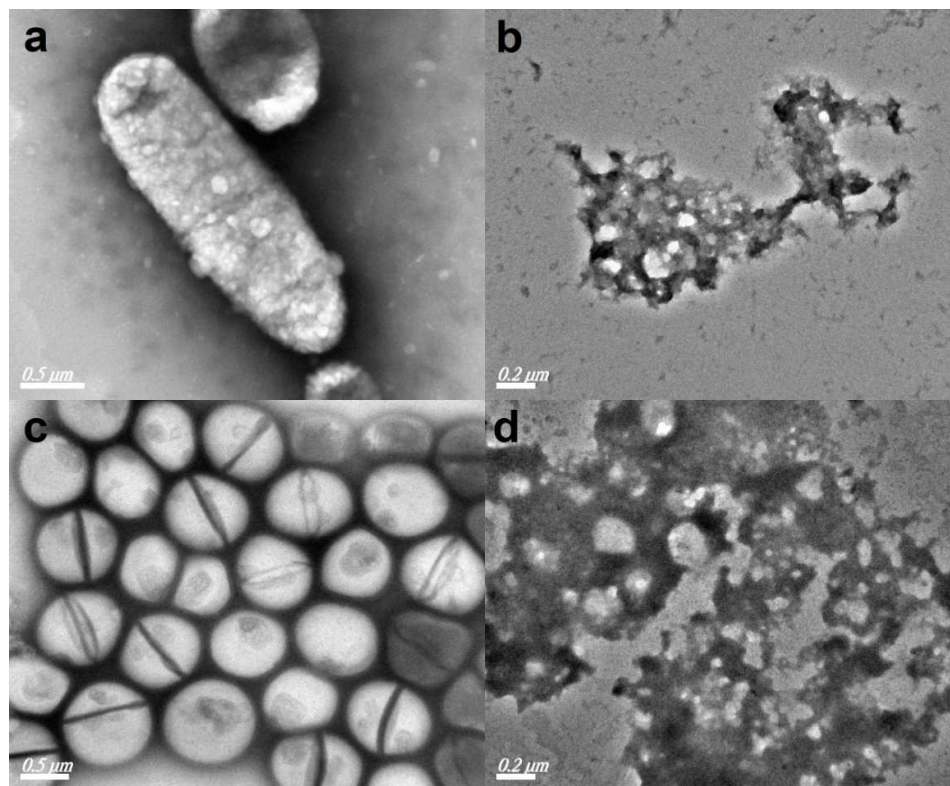
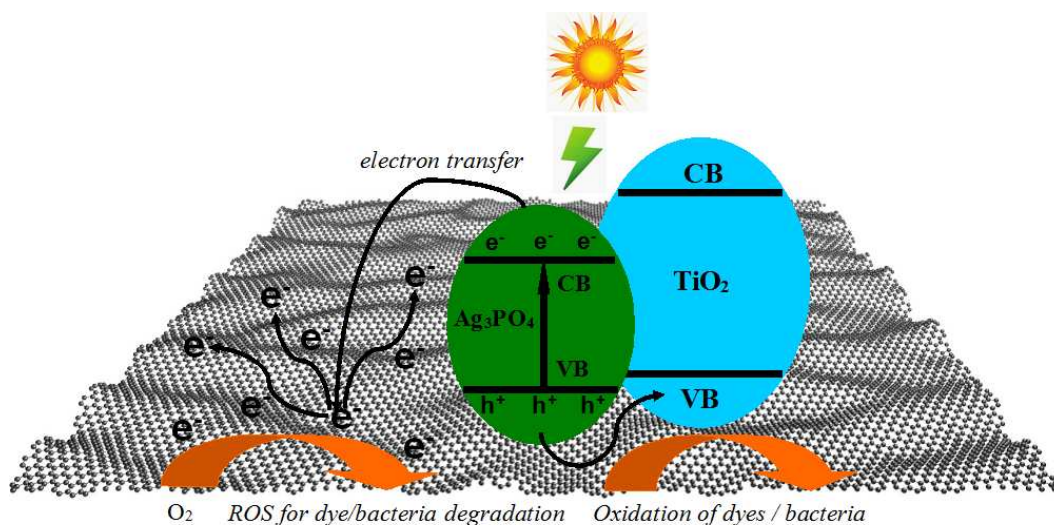


Fig. 5 TEM images of the untreated (a, c) and treated *E. coli* and *S. aureus* cells (b, d)

It is reasonably expected that the as-synthesized three-phase $\text{TiO}_2/\text{Ag}_3\text{PO}_4/\text{GR}$ composite S0.8 displays highly efficient visible-light-driven photocatalytic activity, and demonstrates excellent bactericidal performance against different kinds of bacteria based on the above results and discussion. Due to the presence of graphene and heterogeneous structures, it is necessary to understand possible mechanism for the photocatalytic decoloration of organic dyes and inactivation of bacteria, as a result schematic diagram of the charge separation and transfer in the $\text{TiO}_2/\text{Ag}_3\text{PO}_4/\text{GR}$ composite under visible light irradiation is proposed and is shown in Scheme 2. Generally, several factors are responsible for the enhanced photocatalytic decoloration and bactericidal performance. Firstly, the introduction of GO into the precursor plays an important structure-directing role in the generation of well-defined “pizza-like” $\text{TiO}_2/\text{Ag}_3\text{PO}_4/\text{GR}$ composites. The presence of negatively-charged GO sheets may absorb positively-charged Ag^+ on the large-surface-area GO sheets by the electrostatically-driven assembly. Due to the nature of TiO_2 in a dispersion pH greater than 6, when Degussa P25 was added into the Ag^+ -GO mixture, ultrasonicated TiO_2 nanoparticles can be adsorbed onto the Ag^+ surface. The subsequent addition of PO_4^{3-} results in the formation and the controlled growth of Ag_3PO_4 on the GO

surface, suggesting the construction of well-defined three-phase $\text{TiO}_2/\text{Ag}_3\text{PO}_4/\text{GO}$ structures. The following hydrothermal treatment at 180 °C for 24 h caused little effect on the structure of the composite where the reduction of GO to GR occurs. Compared with pure Ag_3PO_4 , TiO_2 and two-phase $\text{TiO}_2/\text{Ag}_3\text{PO}_4$ composite, as-prepared $\text{TiO}_2/\text{Ag}_3\text{PO}_4/\text{GR}$ composites demonstrate better solubility/dispersibility, which makes primary contribution to the irradiated photocatalytic process and antibacterial experiments under visible light. Secondly, either GO or GR has a large surface area, the $\text{TiO}_2/\text{Ag}_3\text{PO}_4/\text{GR}$ composite exhibits higher adsorption capacity of organic dyes than Ag_3PO_4 , TiO_2 and two-phase $\text{TiO}_2/\text{Ag}_3\text{PO}_4$ composite. Moreover, the presence of black GR in the $\text{TiO}_2/\text{Ag}_3\text{PO}_4/\text{GR}$ composite enhances the absorbance in the visible light region as shown in Fig. 2d. Both the improved adsorption of pollutant/bacteria and effective visible light utilization are helpful to the enhanced photocatalytic performance. Furthermore, most importantly, the formation of the heterostructures is believed to play key roles in the highly efficient photocatalytic performance and antibacterial activities against bacteria. It is well-known that an effective charge separation/transfer is crucial for the enhancement in photocatalytic activities. For the $\text{TiO}_2/\text{Ag}_3\text{PO}_4/\text{GR}$ composite, potentials of both conduction band and valence band of TiO_2 are more negative than those of Ag_3PO_4 (conduction band: 0.45 eV, valence band: 2.45 eV). Under visible light irradiation, TiO_2 nanoparticles possess a large band gap of 3.0 eV that cannot absorb visible light under the present conditions with filtered $\lambda > 420$ nm, the valence band (VB) and the conduction band (CB) of Ag_3PO_4 can be separated easily. Due to the presence of conductive GR sheets, it can serve as an effective acceptor of the photoexcited electrons, hence the photogenerated CB electrons of Ag_3PO_4 can be transferred to GR sheets in the $\text{TiO}_2/\text{Ag}_3\text{PO}_4/\text{GR}$ composite. The transportation and mobility of electrons on GR sheets is very rapid in the specific π -conjugated structure, thus the efficient electron transfer from Ag_3PO_4 to GR sheets keeps electrons away from the Ag_3PO_4 . More photo-generated electrons and holes are produced by continuously working in this way, effectively suppressing the charge recombination and improving the photocatalytic activity. Meanwhile, well-separated electrons in GR sheets can be trapped by the absorbed oxygen in GR surface to generate reactive oxygen species (ROSs) such as superoxide anions (O_2^-), the produced active radical species can decompose dye molecules into CO_2 , H_2O , etc. and attack the specific bacteria. In addition, the photo-induced holes on the surface Ag_3PO_4 particles may

significantly accelerate the photocatalytic degradation of organic dyes or bacteria. It is also confirmed from XRD patterns of different samples before and after recycled photocatalytic experiments in Fig. S3, that the presence of GR in the $\text{TiO}_2/\text{Ag}_3\text{PO}_4/\text{GR}$ composite effectively protects Ag_3PO_4 from being decomposed into metallic Ag, suggesting a better stability and recyclability of $\text{TiO}_2/\text{Ag}_3\text{PO}_4/\text{GR}$ composite in the photocatalytic process.



Scheme 2. Mechanism diagram of photocatalytic degradation of organic dye molecules and bacteria under visible light irradiation.

4. Conclusion

In summary, we have demonstrated an effective hydrothermal approach for the fabrication of $\text{TiO}_2/\text{Ag}_3\text{PO}_4/\text{GR}$ composites. The $\text{TiO}_2/\text{Ag}_3\text{PO}_4/\text{GR}$ composite shows highly efficient photocatalytic degradation activity toward organic dye molecules and also exhibits excellent antibacterial activity against common bacteria. Bifunctional $\text{TiO}_2/\text{Ag}_3\text{PO}_4/\text{GR}$ composites illustrate improved visible light photocatalytic performance and enhanced antibacterial activity compared with bare Ag_3PO_4 , TiO_2 and two-phase composites, due to the generation of composite materials. By adjusting the molar ratio of $\text{Ag}_3\text{PO}_4/\text{TiO}_2$ and the added amount of GO, photocatalytic and antibacterial activities of the composites can be regulated. As a result, this novel bifunctional $\text{TiO}_2/\text{Ag}_3\text{PO}_4/\text{GR}$ composite may finding promising applications in environmental protection and water disinfection.

Acknowledgements

This work was financially supported by the National Natural Science Foundation of China (51102116, 51302112), Natural Science Foundation of Jiangsu (BK2011480, BK2011534).

References

1. J. L. Wang and L. J. Xu, *Crit. Rev. Environ. Sci. Technol.*, 2012, **42**, 251.
2. J. C. Sin, S. M. Lam, A. R. Mohamed and K. T. Lee, *Int. J. Photoenergy*, 2012. Vol. 2012, Article ID 185159, 23 pages, DOI:10.1155/2012/185159.
3. C. P. Silva, M. Otero and V. Esteves, *Environ. Pollut.*, 2012, **165**, 38.
4. B. Limburg, E. Bouwman and S. Bonnet, *Coord. Chem. Rev.*, 2012, **256**, 1451.
5. S. M. Lam, J. C. Sin, A. Z. Abdullah and A. R. Mohamed, *Desalin. Water Treat.*, 2012, **41**, 131.
6. H. Tong, S. X. Ouyang, Y. P. Bi, N. Umezawa, M. Oshikiri and J. H. Ye, *Adv. Mater.*, 2012, **24**, 229.
7. A. Kubacka, M. Fernandez-Garcia and G. Colon, *Chem. Rev.*, 2012, **112**, 1555.
8. Q. J. Xiang, J. G. Yu and M. Jaroniec, *Chem. Soc. Rev.*, 2012, **41**, 782.
9. L. W. Zhang and Y. F. Zhu, *Catal. Sci. Technol.*, 2012, **2**, 694.
10. D. H. Pei and J. F. Luan, *Int. J. Photoenergy*, 2012. Vol. 2012, Article ID 262831, DOI:10.1155/2012/185159.
11. A. Di Paola, E. Garcia-Lopez, G. Marci and L. Palmisano, *J. Hazard. Mater.*, 2012, **211**, 3.
12. E. Casbeer, V. K. Sharma and X. Z. Li, *Sep. Purif. Technol.*, 2012, **87**, 1.
13. X. Q. An and J. C. Yu, *RSC Adv.*, 2011, **1**, 1426.
14. Z. G. Yi, J. H. Ye, N. Kikugawa, T. Kako, S. X. Ouyang, H. Stuart-Williams, H. Yang, J. Y. Cao, W. J. Luo, Z. S. Li, Y. Liu and R. L. Withers, *Nat. Mater.*, 2010, **9**, 559.
15. Y. Bi, S. Ouyang, N. Umezawa, J. Cao and J. Ye, *J. Am. Chem. Soc.*, 2011, **133**, 6490.
16. Y. P. Bi, H. Y. Hu, S. X. Ouyang, G. X. Lu, J. Y. Cao and J. H. Ye, *Chem. Commun.*, 2012, **48**, 3748.
17. Q. H. Liang, W. J. Ma, Y. Shi, Z. Li and X. M. Yang, *CrystEngComm*, 2012, **14**, 2966.
18. Y. P. Bi, H. Y. Hu, Z. B. Jiao, H. C. Yu, G. X. Lu and J. H. Ye, *Phys. Chem. Chem. Phys.*, 2012, **14**, 14486.
19. Z. B. Jiao, Y. Zhang, H. C. Yu, G. X. Lu, J. H. Ye and Y. P. Bi, *Chem. Commun.*, 2013, **49**, 636.
20. J. Wang, F. Teng, M. D. Chen, J. J. Xu, Y. Q. Song and X. L. Zhou, *CrystEngComm*, 2013, **15**, 39.
21. W. F. Yao, B. Zhang, C. P. Huang, C. Ma, X. L. Song and Q. J. Xu, *J. Mater. Chem.*, 2012, **22**, 4050.
22. R. Y. Liu, P. G. Hu and S. W. Chen, *Appl. Surf. Sci.*, 2012, **258**, 9805.
23. S. B. Rawal, S. D. Sung and W. I. Lee, *Catal. Commun.*, 2012, **17**, 131.
24. G. P. Li and L. Q. Mao, *RSC Adv.*, 2012, **2**, 5108.
25. L. L. Zhang, H. C. Zhang, H. Huang, Y. Liu and Z. H. Kang, *New J. Chem.*, 2012, **36**, 1541.

26. Y. P. Liu, L. Fang, H. D. Lu, L. J. Liu, H. Wang and C. Z. Hu, *Catal. Commun.*, 2012, **17**, 200.
27. Y. P. Liu, L. Fang, H. D. Lu, Y. W. Li, C. Z. Hu and H. G. Yu, *Appl. Catal. B*, 2012, **115**, 245.
28. Y. P. Bi, H. Y. Hu, S. X. Ouyang, Z. B. Jiao, G. X. Lu and J. H. Ye, *J. Mater. Chem.*, 2012, **22**, 14847.
29. Y. P. Bi, H. Y. Hu, S. X. Ouyang, Z. B. Jiao, G. X. Lu and J. H. Ye, *Chem. Eur. J.*, 2012, **18**, 14272.
30. W. Teng, X. Y. Li, Q. D. Zhao, J. J. Zhao and D. K. Zhang, *Appl. Catal. B*, 2012, **125**, 538.
31. Y. Hou, F. Zuo, Q. Ma, C. Wang, L. Bartels and P. Y. Feng, *J. Phys. Chem. C*, 2012, **116**, 20132.
32. J. Cao, B. D. Luo, H. L. Lin, B. Y. Xu and S. F. Chen, *J. Hazard. Mater.*, 2012, **217**, 107.
33. Y. P. Bi, S. X. Ouyang, J. Y. Cao and J. H. Ye, *Phys. Chem. Chem. Phys.*, 2011, **13**, 10071.
34. Q. H. Liang, Y. Shi, W. J. Ma, Z. Li and X. M. Yang, *Phys. Chem. Chem. Phys.*, 2012, **14**, 15657.
35. L. Liu, J. C. Liu and D. D. Sun, *Catal. Sci. Technol.*, 2012, **2**, 2525.
36. G. D. Chen, M. Sun, Q. Wei, Y. F. Zhang, B. C. Zhu and B. Du, *J. Hazard. Mater.*, 2013, 244-245, 86.
37. H. C. Zhang, H. Huang, H. Ming, H. T. Li, L. L. Zhang, Y. Liu and Z. H. Kang, *J. Mater. Chem.*, 2012, **22**, 10501.
38. X. T. Hong, X. H. Wu, Q. Y. Zhang, M. F. Xiao, G. L. Yang, M. R. Qiu and G. C. Han, *Appl. Surf. Sci.*, 2012, **258**, 4801.
39. J. J. Buckley, A. F. Lee, L. Olivi and K. Wilson, *J. Mater. Chem.*, 2010, **20**, 8056.
40. H. Y. Cui, X. F. Yang, Q. X. Gao, H. Liu, Y. Li, H. Tang, R. X. Zhang, J. L. Qin and X. H. Yan, *Mater. Lett.*, 2013, 93, 28.
41. X. F. Yang, H. Y. Cui, Y. Li, J. L. Qin, R. X. Zhang and H. Tang, *ACS Catal.*, 2013, 3, 363.
42. D. C. Marcano, D. V. Kosynkin, J. M. Berlin, A. Sinitiskii, Z. Z. Sun, A. Slesarev, L. B. Alemany, W. Lu and J. M. Tour, *ACS Nano*, 2010, 4, 4806.
43. X. F. Yang, H. Y. Ding, D. Zhang, X. H. Yan, C. Y. Lu, J. L. Qin, R. X. Zhang, H. Tang and H. J. Song, *Cryst. Res. Technol.*, 2011, 11, 1195.